Optimization of thermoelectric properties achieved in Cu doped β-In_2S_3 bulks

Yue-Xing Chen,[a] Fu Li,[a]* Wenting Wang,[a] Zhuanghao Zheng,[a,b] Jingting Luo,[a]

Ping Fan,[a]* Tsunehiro Takeuchi[c]

a Shenzhen Key Laboratory of Advanced Thin Films and Applications, College of Physics and Energy, Shenzhen University, Shenzhen, 518060, China.

b Laboratory of Glasses and Ceramics, Institute of Chemical Science UMR CNRS6226,University of Rennes 1, Rennes 35042, France

c Toyota Technological Institute, Nagoya, 468-8511, Japan

** Corresponding authors; Emails:lifu@szu.edu.cn； fanping@szu.edu.cn*

Abstract

β-$In_{2-x}Cu_xS_3$ ($0 \leq x \leq 0.40$) bulks were prepared by solid-state reaction followed by pulsed current sintering. For $x \leq 0.20$, X-ray diffraction indicated the formation of single phase, while the secondary phase, Cu_2S, was observed for the samples prepared at x = 0.30 and x = 0.40. The Cu-doping allowed us to optimize the power factor in range of whole measured temperature by reducing the low temperature electrical resistivity. With the significant reduction in lattice thermal conductivity, a maximum ZT of 0.51 at 700 K and an average ZT of 0.31 from 300 to 700 K were obtained for the sample with x= 0.05, which values are 0.3 and 1.2 times higher than that of pristine sample.

Key words: Thermoelectric, doping effect, thermal conductivity, β-In_2S_3

1. Introduction

Thermoelectric (TE) generators, which directly convert waste heat into useful electrical energy, have attracted increasing attention in recent decades.[1-2] The performance of TE materials are usually appraised by the dimensionless figure of merit defined as $ZT = S^2T\rho^{-1}\kappa^{-1}$, where S, ρ, κ, and T represent Seebeck coefficient, electrical resistivity, thermal conductivity and absolute temperature, respectively. The coupling among three parameters of S, ρ and κ has hindered the dramatically enhancement of ZT. To greatly enhance ZT values, TE scientists have made efforts to decouple them through two major strategies: (a) optimizing the carrier concentration n [3-5] under the band engineering [6-8] for achieving high power factor $PF = S^2/\rho$, and (b) nanostructure engineering to reduce κ without sacrificing the electrical transport properties. [9-11]

Some new chalcogenides, such as SnSe, SnS, Bi_2S_3, Cu_2S, and In_2Se_3, had already developed as promising TE materials.[4,12-19] These compounds are known to possess very low lattice thermal conductivity which majorly contributes to an effective increase of the value of ZT higher than unity. For example, the thermoelectric properties of both single and polycrystalline SnSe have been investigated widely and extremely high ZT values were reported.[4,19-24] The extraordinarily low lattice thermal conductivity about 0.2 - 0.3 $Wm^{-1}K^{-1}$ was found in both *p*- and *n*- type SnSe crystals to realize the extremely high ZT values larger than 2.5. [4, 20-21]

Besides, α-In_2Se_3 is another typical chalcogenide with low lattice thermal conductivity $\kappa_L \sim 0.8$ $Wm^{-1}K^{-1}$ at room temperature. [14, 26-27] After the appropriate element doping, the κ_L was reported to be decreased to extremely low value of ~ 0.3 Wm^{-}

$^{1}K^{-1}$ at 916 K leading to a maximum *ZT* of 1.24 at the same temperature.[26-27] However, toxic chemical component Se of α-In_2Se_3 restricts its further application development.

Recently, β-In_2S_3 compounds which consist of cheaper and nontoxic sulfur are investigated as a good TE candidate due to the low lattice thermal conductivity and decent electrical transport properties.[28,29] β-In_2S_3 with space group of $I4_1/amd$ is stable at the room temperature. As temperature increases, the β-In_2S_3 transforms into α-In_2S_3 (space group:$Fd\bar{3}m$) at 693 K and then to γ- In_2S_3 (space group: $P\bar{3}m1$) at 1027 K.[30] In our previous work, we reported that *n*-type bulk sample of β-In_2S_3 prepared by conversional solid state reaction method and pulsed current sintering achieved a maximum *ZT* of 0.38 at 700 K.[28] The first principles band calculations and simulation of electron transport properties with semi-classical Boltzmann transport equation predicted that *p*-type β-In_2S_3 may possess a larger *ZT* value of 1.4 with an appropriate carrier concentration. [28] This fact suggests that β-In_2S_3 is a very promising TE material, despite that *p*-type samples are hardly obtainable because of the bonding nature of valence band edge to generate S deficiency during the material synthesis.

More recently, we employed alkali element Mg, which possesses less number of valence electrons than In, as the partial substitute for Into generate hole carriers. [29] However, the prepared Mg doped β-In_2S_3 bulks in various doping amount still showed *n*-type behavior in range of whole measured temperature. With a small amount of Mg doping, the number of conduction electrons was somehow reduced to increase the magnitude of Seebeck coefficient and electrical resistivity, but we did not reached *p*-type condition within the solubility limit of Mg.

Notably, however, the significant reduction of thermal conductivity brought about by the Mg doping contributed for an increase of *ZT* up to 0.53 at 700 K indicating the potential of enhancement in *ZT* by element doping. Besides, few works were reported about the doping of other elements to realize *n*-type β-In_2S_3. In this work, therefore, we further investigated the TE properties of β-In_2S_3 by employing Cu-doping. The element dependence of doping effects on thermoelectric properties are discussed in comparison with the rigid band model.

2. Experimental

2.1 Synthesis

Pristine β-In_2S_3 and Cu doped β-In_2S_3 were synthesized by means of conventional solid-state reaction. High purity elements, In (99.99%, Grains), S (99.99%, Powder) and Cu (99.9%, Powder), were weighed in the atomic ratio of In: Cu : S = 2-x : x : 3 (x = 0, 0.05, 0.10, 0.15, 0.20, 0.30, and 0.40) and sealed in a quartz tube with vacuum atmosphere of about 1×10^{-3} Pa. The quartz tube was heated up to 673 K in 2 hours, then slowly heated up again to 773 K spending 10 hours to avoid the rapidly evaporation of S. In the third step, the quartz was heated up to 973 K and kept at this temperature for 24 h, then slowly cooling in the furnace down to the room temperature. The obtained ingot was pulverized into powders, and consolidated again by means of pulsed current sintering (PCS) at 873 K with a pressure of 30 MPa. For comparison the element doping effects, stoichiometric Ag doped ($In_{1.8}Ag_{0.2}S_3$) , Mg doped ($In_{1.8}Mg_{0.2}S_3$), Sb doped ($In_{1.8}Sb_{0.2}S_3$) and Mg&Sb co-doped ($In_{1.6}Mg_{0.2}Sb_{0.2}S_3$) samples are also prepared by the same process.

2.2 Characterization

The powder and bulk X-ray diffraction (XRD) patterns were measured to determine the phases involved in the prepared compounds over the 2θ range from 10° to 60° by using Bruker D8 Advanced diffractometer with Cu Kα radiation. The microstructure and composition of bulk sample were analyzed using Field Emission Scanning Electronic Microscopy (FESEM), and Energy Dispersive X-ray Spectroscopy (EDS) (Supra55 Sapphire, Zeiss, Germany).

Measurements of S and ρ were performed in a vacuum atmosphere from 300 to 700 K with a commercial Seebeek Measurement System, manufactured by MMR technology, and a standard four-probe method, respectively. The thermal diffusivity D was measured on the disk-shaped pellets of Φ10 mm × t 1.0 mm in dimension using a laser flash method (LFA 457 Microflash, Netzsch, Germany) from 300 to 773 K. The thermal conductivity was calculated by use of the relationship $\kappa = D \times C\text{p} \times d$, where Cp is the specific heat which was derived using a representative sample of Pyroceram 9606 and the d is the density of the sample measured by Archimedes method.

3. Results and Discussion

Fig. 1a shows the powder XRD patterns for bulk samples $In_{2-x}Cu_xS_3$ ($0 \leq x \leq 0.40$) in different doping amount of Cu. All the samples are corresponding to the calculation pattern of β-In_2S_3 phase,[31] which means the main phase was kept unchanged for all samples after the sintering process. Fig. 1b displays the magnified view of (109) peak at 2θ range from 27◦ to 28◦. Compare to the pristine β-In_2S_3 samples, all the peaks for Cu doped samples shift to higher angle, indicating the substitution of smaller Cu in the sites of larger In in the β-In_2S_3 phase. This fact is also confirmed by the variation of lattice

parameters and volume of unit cell as shown in Fig.2. The covalent radius of Cu^{+} (0.96 Å) and Cu^{2+}(0.72 Å) is also smaller than that of In^{3+} (1.44 Å) which naturally led to the decreasing lattice constant with increasing Cu content. With increasing Cu content up to x = 0.20, the peaks were continuously moved to higher angles suggesting the formation of solid solution. For $x \geq 0.30$, some additional peaks of secondary phase(s) were observed at $2\theta \sim 27.8°$. This fact indicates that the solubility limit of Cu in β-In_2S_3 is less than x = 0.3.

The XRD patterns for the samples with x = 0.30 and x = 0.40 around the peaks of (3 0 9) and (2 2 12) shown in Fig.1c also proved the precipitation of second phase(s). As compared with the standard data base for all the possible related compounds, we identified the secondary phase as cuprous sulfide (Cu_2S, PDF#53-0522). The appearance of Cu_2S greatly impacted the TE properties which will be discussed later.

Fig. 2 shows the lattice parameters and the unit cell volume plotted as a function of nominal Cu content for $In_{2-x}Cu_xS_3$ ($0 \leq x \leq 0.40$). In this figure, the structure variation caused by introducing Cu was roughly understood. The crystal structure of β-In_2S_3 is tetragonal with long c axis about 32.30 Å and short a and b axis about 7.62Å in the pristine sample. With increasing Cu content, a decreased from 7.62 Å for x = 0 to 7.55 Å for x = 0.30, and then increase again for x = 0.40 most likely because the precipitation of secondary phase changed the composition of main phase in x = 0.4 different from x = 0.3. The reduction of lattice parameter a would be caused by the substitution of smaller Cu for larger In. However, the lattice parameter c showed weak but non-trivial behavior to be almost constant over the whole Cu concentration. This fact is difficult to understood as a result of Cu-substitution for In, and therefore some structure variations different from the

simple substitution of Cu for In are suggested. This point will be discussed in more detail with the variation of electron transport properties.

Combining with the results of XRD patterns and lattice parameter variation, we safely draw a conclusion that the solid solubility limit of Cu in β-In_2S_3 matrix is smaller than 0.30, which is different from the Mg doped samples reported in our previous work. [29]

Fig.3a displays the back-scattered electron image for Cu doped β-In_2S_3 with x = 0.10. Precipitation of secondary phases was not observed, showing a good consistency with the XRD pattern in Fig. 1. The corresponding element-mappings for In, S and Cu on the polished surface were observed for a representative sample (x = 0.10) and displayed in Fig. 3b-d. In, S and Cu were homogeneously distributed, and no evidence was observed for the formation of secondary phase. We also determined the chemical composition using EDS and found that In- and S- concentrations were 40.1 at.% and 58.8 at.%, respectively. These numbers indicated that S deficiency was also unavoidable in this work as those in our previous work [28-29].

Fig. 4 shows the temperature dependence of Seebeck coefficient S, electrical resistivity ρ and power factor PF measured for $In_{2-x}Cu_xS_3$ ($0 \leq x \leq 0.40$) samples. Generally speaking, the precipitation of secondary phase would greatly deteriorate the electrical transport properties, therefore, we only measured the TE properties for the single-phase samples obtained in the composition range of $0 \leq x < 0.30$. The negative sign of Seebeck coefficient for all the samples, as shown in Fig.4a, indicated that the

major carrier is still electrons even after introducing Cu in the same manner as that in the Mg doped samples.

With increasing Cu content, the absolute value of *S* at room temperature decreased, the value from 220 μVK^{-1} for x = 0 decreased to 190 μVK^{-1} for x = 0.05 and ~ 130 μVK^{-1} for x = 0.10 and 0.20. The temperature dependence of *S* is quite similar with x = 0; that is monotonically increased up the 600 K achieving a maximum value. [28] The absolute value of Seebeck coefficient |*S*| decreased with increasing Cu concentration up to x = 0.20 at room temperature which may indicate the increase of *n*-type carriers: electrons. Since Cu-substitution for In, which was confirmed from the lattice constant and unit cell volume, naturally leads to a reduction of electron concentration, some other factors increasing electron concentration should be considered. One of the possible mechanism for the unusual Cu-concentration dependence of *S* is the filling of Cu atoms in the naturally existing 'vacancy-sites' of β-phase [28, 32]. Another possible factor is the formation of sulfur defects. Notably, both factors lead to an effective increase of conduction electrons. Once these effects were saturated, the effect of Cu-substitution for In became obvious to reduce the electron concentration, and the sample of x = 0.3 showed almost the same behavior of Seebeck coefficient as that of x = 0.05.

Cu concentration dependence of electrical resistivity also supports this scenario which will be discussed later. The electronic structure calculations suggested that the nature bonding between 3*p* orbits of sulfur atoms and 5*d* orbits of indium near valence band maximum (VBM) would prevent us from easily introducing holes in β-In_2S_3,[28] and that the deficiency of sulfur compensates the reduction of electrons by Mg-doping. In this work, the carrier type is maintained to be electrons due to the deficiency of sulfur as

detected by EDS, and the same mechanism was supposed to be realized in other Cu or Cd doped β-In_2S_3 single crystals. [33]

Fig. 4b shows the temperature dependence of electrical resistivity for β-$In_{2-x}Cu_xS_3$ ($0 \leq x \leq 0.30$). The ρ at 300 K became getting smaller with increasing Cu concentration up to $x = 0.20$. This fact is definitely consistent with the variation in S in terms of carrier concentration variation. For $x = 0.30$, the room temperature electrical resistivity was turned up to increase to about 0.27 Ωcm which is several times higher than that of other Cu doped samples. At the Cu concentration range of $0.05 \leq x \leq 0.20$, the electron concentration was increased with increasing Cu because the Cu atoms filled the vacant sites or the S-defects created. After taking maximal electron concentration, it turned out to decrease presumably because Cu-substitution for In stated to have a dominant effect.

The temperature dependence of electrical resistivity also changed with Cu doing. The ρ (T) for $x = 0$ had described to follow the Mott's variable range hopping (VRH) conduction mechanism generally observable for the states under the Anderson localization. [28, 34] Note here that Anderson localization takes places when the highly disorder structure is realized with small electrical density of states in the vicinity of Fermi energy. As shown in the inset of Fig.4b, ρ of Cu doped samples no longer showed any decreasing tendency with increasing temperature, but gradually increased at the almost whole measurement temperature range and kept constant above 600 K. This may indicate that increased number of carriers in association with the Cu-filling in the vacant sites and/or S-defects formation destroyed the localized states, and the itinerant states were recovered to possess metallic electrical conduction. The localization tendency of conduction electrons was again observable at $x = 0.3$, where the electron concentration

was effectively reduced due to the monovalent Cu-substitution for tri-valent In. The degree of disordering in x = 0.3 was supposed to be much severe than that in pristine sample, and therefore the localization tendency became more obvious in x = 0.3. The change in localized states near the bottom conduction band which is governed by $s - p$ orbits after Cu doped. To figure out this problem, some theoretical calculations should be performed in the future.

Combining with the variation at S and ρ discussed above, the calculated PF is plotted as a function of temperature in Fig.4c. The $PF(T)$ shows weaker temperature dependence for Cu doped samples. Especially, for x = 0.05, the room temperature PF is about 380 $\mu Wm^{-1}K^{-2}$ which is six times higher than that of x = 0, and the value increases to about 600 $\mu Wm^{-1}K^{-2}$ around 450 K. This result sufficiently proved the potential of β-In_2S_3based compound as a good TE material.

The thermal conductivity of Cu doped β-In_2S_3 as a function of temperature are shown in the Fig.5. The measured thermal conductivity κ for x = 0 was about 1.6 $Wm^{-1}K^{-1}$ at room temperature and gradually decreases with increasing temperature. The value of κ(300 K) also decreases with increasing Cu-concentration, and it reached a half value of pristine sample at x = 0.20 and x = 0.30, despite that metallic electrical conduction recovered at larger x-values. This great reduction in thermal conductivity is attributed to the reduction of lattice thermal conductivity caused by the disordering in association with the Cu doping.

For further investigating the effect of Cu doping on the transport of phonons, we roughly eliminated the electrical thermal conductivity κ_{el} from the measured data using the well-known Wiedemann–Franz law, $\kappa_{el} = LT/\rho$, where L represents a constant known

as the Lorenz number: 2.44 $\times 10^{-8}$ $W^{-1}K^{-2}$. The variation of κ_{el} and κ_L are plotted as a function of temperature in Fig.5b. The magnitude of κ_{el} show in Fig.5c were kept small over the entire temperature range of measurement, even though the resistivities had been effectively decreased by the Cu doping. This fact definitely indicated that the thermal conductivity was dominated by κ_L.

The very small magnitude of κ_{lat} of all the samples especially at high temperatures wound be caused by the strong anharmonicity in lattice vibrations, that was also observed in other chalcogenides. [12-21] With increasing Cu-concentration, the κ_L at room temperature decreases from 1.2 $Wm^{-1}K^{-1}$ for x = 0.05 to 0.8 $Wm^{-1}K^{-1}$ for x = 0.20 and x = 0.30 because of the increasing degree of structure and/or chemical disorderings. Notably, the differences become smaller as the temperature rises most likely due to the excited phonons at high temperatures smeared the static structure disordering. The curve of $\kappa_{lat}(T)$ for x = 0.30 is almost overlapped with that of x = 0.20 in range of whole measured temperature, which might indicate that the position of additional Cu atoms at x = 0.30 was different from that in the samples of $x \leq 0.2$.

With the electrical and thermal transport experimental data plotted above, we deduced the *ZT* values for $In_{2-x}Cu_xS_3$ ($0 \leq x \leq 0.30$) and plotted in Fig.6a. Due to the synergistic optimization of electrical transport properties and reduction in κ_{lat} caused by point defect scattering after Cu doping, the *ZT* values at 300 K for samples at low doping level (x = 0.05 and x = 0.10) significantly improve to 0.09 and 0.05, respectively. While other two samples show lower values than pristine one as their *PF* are uncompetitive. For x = 0.05, the *ZT* value gradually arises with the temperature from 0.09 at 300 K to 0.51 at 700 K, the maximum value of *ZT*, which is denoted as ZT_{max}, became 30 % higher than that of

the pristine sample and comparable with Mg doped samples.

To evaluate the application prospect as a TE material, the average value of *ZT*, which is hereafter denoted as ZT_{ave}, is considered, because ZT_{ave} must be a more important parameter than ZT_{max} for the material performance in real applications. In Fig. 6b, we compare the ZT_{max} and ZT_{ave} (from 300 to 700 K) of Mg doped and Cu doped samples which perform the best TE properties with pristine β-In_2S_3 sample. The ZT_{max} is generally improved up to 0.5 after doping with Mg and Cu. This fact suggests that the doping at In-sites is a good way to optimize the TE performance. In sharp contrast to no improvement of the ZT_{ave} for the Mg, the ZT_{ave} for Cu doped sample reaches 0.31, that is more than two times larger than that of pristine and Mg doped samples. This result indicates that the Cu doping is a more preferable to improve the TE performance of β-In_2S_3.

To further improve the TE properties of β-In_2S_3, we discuss here the strategies via element doping. By now, we revealed that Mg and Cu-doping effectively improve the thermoelectric performance of β-In_2S_3. To further understand the difference between Mg and Cu doping, we compared the room temperature TE properties among the pristine sample, Mg doped and Cu doped samples on Table 1. As shown in the table, electrical resistivity is more sensitive to the doping elements than that of Seebeck coefficient. The sign of Seebeck coefficient is kept negative even employing the *p*-type doping due to the unavoidable S deficiency or the filling of vacancies. It is reported in previous work, the valence band near the gap is mainly composed of 3*p* orbitals of *S* atoms 5*d* orbitals and the corresponding anti-bonding bands exist in the conduction band at above 1.5 eV. Hence, to optimize the transport properties of the β-In_2S_3, the doping elements should

make change on the bonding nature of conduction and valence band. By knowing that Cu doping greatly affect the electrical transport properties on pristine samples, we consider that the transition metal elements having the similar electron configuration with Cu will be appropriate as doping elements.

Another strategy to enhance *ZT* is to reduce the thermal conductivity. As shown in Table 1, the room temperature κ was significantly decreased with the substituted or doped atoms. This encouraged us to try different element doping on both In and S sites. Figure7 shows thermal conductivity of samples with different doping elements. Even with the same doping amount, the reduction of κ varied with elements. Comparing with the Cu doped samples referred above, Mg and Ag doped samples definitely show higher values of κ, while Sb-doped samples and (Mg, Sb) co-doped samples show lower magnitude of κ. It's worth noting that Sb-doping and (Mg, Sb) co-doping achieved an extremely low κ about $0.5 Wm^{-1}K^{-1}$ at room temperature which was lower than that of most of the state of art TE materials. The relatively low thermal conductivity may attribute to introduction of heavy element Sb which is easier to be scatter center and hindering the propagation of heat. Unfortunately, however, the great reduction in κ for Sb doping and (Mg, Sb) co-doping samples did not bring any significant increase of *ZT* due to their poor electrical transport properties.

From the facts mentioned above, we consider that further optimization of TE performance for β-In_2S_3 is possible through Sb and Cu co-doping because both of electrical and thermal transport properties might significantly optimized in a very wide temperature range. To realize this, more theoretical calculations and experiments should be done in the future.

4. Conclusion

β-$In_{2-x}Cu_xS_3$ ($0 \leq x \leq 0.40$) bulks were prepared by solid-state reaction method and were sintered with pulsed current sintering technique. Secondary phase of Cu_2S was observed by X-ray diffraction when the doping exceeds 0.30. Cu doping brought two effects: significantly decreased in low temperature electrical resistivity which led to the optimization of power factor in range of whole measured temperature, and reduction inlattice thermal conductivity due to the increasing degree of disordering. As a result, ZT_{max} of 0.51 at 700 K and ZT_{ave} of 0.31 from 300 to 700 K were obtained for the sample with x= 0.05. The ZT_{ave} is 1.3 times higher than that of pristine and Mg doped samples indicating Cu doping is more efficiently way to optimize the TE performance of β-In_2S_3. Hence, through element doping to further optimization of TE performance for β-In_2S_3 is possible as both of electrical and thermal transport properties can be significantly optimized in a very wide range.

Acknowledgements

This work was supported by the Fund of Natural Science Foundation of Guangdong Province (no.2018A030313574) and Shenzhen Science and Technology Plan Project (no.JCYJ20170818142740568, JCYJ20160422102622085).

Reference

[1] L. E. Bell, Cooling, heating, generating power, and recovering waste heat with thermoelectric systems, Science 321 (2008) 1457-1461.

[2] J. F. Li, W. S. Liu, L. D. Zhao, M. Zhou, High-performance nanostructured thermoelectric materials, NPG Asia Mater. 2 (2010) 152-158.

[3] Y. Pei, Z. M. Gibbs, A. Gloskovskii, B. Balke, W. G. Zeier, G. J. Snyder, Optimum carrier concentration in n-type PbTe thermoelectrics, Adv. Energy Mater. 4 (2014) 1400486.

[4]L.-D. Zhao, G. Tan,S. Hao, J. Q. He, Y. Pei, H. Chi, H. Wang, S. Gong, H. Xu, V. Dravid, C. Uher, J. Snyder, M. G. Kanatzidis, Ultrahigh power factor and thermoelectric performance in hole-doped single-crystal SnSe, Science 351 (2016) 141-144.

[5] Z. G. Chen, G. Han, L. Yang, L. Cheng, J. Zou, Nanostructured thermoelectric materials: current research and future challenge, Prog. Nat. Sci. 22 (2012) 535-549.

[6] Y. Pei, A. LaLonde, S. Iwanaga, G. J. Snyder, High thermoelectric figure of merit in heavy-hole dominated PbTe, Energy Environ. Sci. 4 (2011) 2085-2089.

[7] Z. H. Ge, Y. X. Zhang, D. Song, X. Chong, P. Qin, F. Zheng, J. Feng, L. D. Zhao, Excellent *ZT* achieved in $Cu_{1.8}S$ thermoelectric alloys through introducing rare-earth trichlorides, J. Mater. Chem. A 6 (2018) 1444 -14448.

[8] H. Wu, C. Chang, D. Feng, Y. Xiao, X. Zhang, Y. Pei, S. Gong, J. He, M. G. Kanatzidis, L.-D. Zhao, Synergistically optimized electrical and thermal transport

properties in SnTe via alloying high-solubility MnTe, Energy Environ. Sci. 8 (2015) 3298-3312.

[9] C. Gayner, K. K. Kar, Recent advances in thermoelectric materials, Prog. Mater. Sci. 83 (2016) 330-382.

[10] Q. H. Zhang, X. Y. Huang, S. Q. Bai, X. Shi, C. Uher, L. D. Chen, Thermoelectric devices for power generation: recent progress and future challenges, Adv. Eng. Mater. 18 (2016) 194-213.

[11] J. P. Heremans, M. S. Dresselhaus, L. E. Bell, D. T. Morelli, When thermoelectrics reached the nanoscale, Nat. Nanotechnol. 8 (2013) 471-473.

[12] Asfandiyar, Z. L. Li, F. H. Sun, H. C. Tang, J. F. Dong, J. F. Li, Enhanced thermoelectric properties of p-type $SnS_{0.2}Se_{0.8}$ solid solution doped with Ag, J. Alloy Compd. 745 (2018) 172-178.

[13] D. Li, X. Y. Qin, H. J. Zhang, H. H. Hoon, The effects of high-pressure compression on transport and thermoelectric properties of TiS_2 at low temperatures from 5 to 310 K, J. Appl. Phys. 103 (2008) 123704.

[14] J. Cui, L. Wang, Z. Du, P. Ying, Y. Deng, High thermoelectric performance of a defect in α-In_2Se_3-based solid solution upon substitution of Zn for In, J. Mater. Chem. 3 (2015) 9069-9075.

[15] Q. Tan, J.-F. Li, Thermoelectric Properties of Sn-S Bulk materials prepared by mechanical alloying and spark plasma sintering J. Electron. Mater. 43 (2014) 2435-2439.

[16] Z. H. Ge, P. Qin, D. S. He, X. Chong, D. Feng, Y. H. Ji, J. Feng, J. He, Highly Enhanced Thermoelectric Properties of Bi/Bi_2S_3 Nanocomposites, ACS Appl. Mater. Interfaces 9 (2017) 4828 - 4834.

[17] K. Suekuni, K. Tsuruta, T. Ariga, M.Koyano, Thermoelectric properties of mineral tetrahedrites $Cu_{10}Tr_2Sb_4S_{13}$ with low thermal conductivity, Appl. Phys. Express 5 (2012) 051201.

[18] Y. He, T. Day, T. Zhang, H. Liu, X. Shi, L. Chen, G. J. Snyder, High thermoelectric performance in non-toxic earth-abundant copper sulfide, Adv. Mater. 26 (2014) 3974-3978.

[19] Z. H. Ge, Y. H. Ji, Y. Qiu, X. Chong, J. Feng, J. He, Enhanced thermoelectric properties of bismuth telluride bulk achieved by telluride-spilling during the spark plasma sintering process, Scripta Mater. 143 (2018) 90- 93.

[20] L.-D. Zhao, S.-H. Lo, Y. Zhang, H. Sun, G. Tan, C. Uher, C. Wolverton, V. P. Dravid, M. G. Kanatzidis, Ultralow thermal conductivity and high thermoelectric figure of merit in SnSe crystals, Nature 508 (2014) 373-377.

[21] C. Chang, M. Wu, D. He, Y. Pei, C. Wu, X. Wu, H. Yu, F. Zhu, K. Wang, Y. Chen, L. Huang, J. Li, J. Q. He, L.D. Zhao, 3D charge and 2D phonon transports leading to high out-of-plane *ZT* in n-type SnSe crystals, Science 360 (2018) 778-783.

[22] F. Li, W. Wang, X. Qiu, Z. Zheng, P, Fan, J. Luo, B. Li, Optimization of thermoelectric properties of n-type Ti, Pb co-doped SnSe, Inorg. Chem. Front. 4 (2017) **4**, 1721-1729.

[23] X. Q. Huang, Y. X. Chen, M. Yin, D. Feng, J. He, Origin of the enhancement in transport properties on polycrystalline SnSe with compositing two-dimensional material $MoSe_2$, Nanotechnology 28 (2017) 105708.

[24] H. Ju, M. Kim, D. Park, J. Kim, A strategy for low thermal conductivity and enhanced thermoelectric performance in SnSe: porous $SnSe_{1-x}S_x$ nanosheets, Chem. Mater. 29 (2017) 3228-3236.

[25] T. R. Wei, G. Tan, C. F. Wu, C. Chang, L. D. Zhao, J. F. Li, G. J. Snyder, M. G. Kanatzidis, Thermoelectric transport properties of polycrystalline SnSe alloyed with PbSe, Appl. Phys. Lett.110 (2017) 053901.

[26] Z. Song, J. Liu, Z. Du, X. Liu, J. Cui, Improvement of thermoelectric performance of α-In_2Se_3 upon S incorporation, Phys. Status Solidi A 213 (2016) 986-993.

[27] Q. Wang, L. Yang, S. Zhou, X. Ye, Z. Wang, W. Zhu, M. D. McCluskey, Y. Gu, Phase-defined van der Waals schottky Junctions with significantly enhanced thermoelectric properties, J. Phys. Chem. Lett. 8 (2017) 2887-2894.

[28] Y.X. Chen, K. Kitahara, T. Takeuchi, Thermoelectric properties of b-Indium sulfide with sulphur deficiencies, J. Appl. Phys. 118 (2015) 245103..

[29] Y. X. Chen, A. Yamamoto, T. Takeuchi, Doping effects of Mg for In on the thermoelectric properties of β-In_2S_3 bulk samples, J. Alloys Compd. 695 (2017) 1631-1636.

[30] V. G. Bessergenev, E. N. Ivanova, Y. A. Kovalevskaya, S. A. Gromilov,V. N. Kirichenco, S. V. Larionov, V.G. Bessergenev, E.N. Ivanova, Y.A. Kovalevskaya, S.A.

Gromilov,Electrical properties of conductive In_2S_3 and In_2O_3[S] films prepared from the In(S2COC3H7-iso)(3) volatile precursor, Inorg. Mater. 32 (1996) 592-596.

[31] G.A. Steigmann, H.H. Sutherl, J. Goodyear, The crystal structure of β-In_2S_3, Acta Cryst. 19 (1965) 967-971.

[32] R. S. Becker, T. Zheng, J. Elton, M. Saeki, Synthesis and photoelectron chemistry of In_2S_3, Solar Energy Mater.13 (1986) 97-107.

[33] W.Rehwald, G. Harbeke, On the conduction mechanism in single crystal β-indium sulfide In_2S_3, J. Phys. Chem. Solids 26 (1965) 1309-1324.

[34] N. F. Mott, Conduction in non-crystalline materials. 3. localized states in a pseudo gap and near extremities of conduction and valence bands, Philos. Mag. 19 (1969) 835-852.

Figure captions

Fig. 1 (a) Powder XRD patterns for bulk sample of $In_{2-x}Cu_xS_3$ ($0 \leq x \leq 0.40$) and (b) expand view of patterns with 2θ range from 27◦-28◦; (c) expand view of patterns with 2θ range from 40◦-52◦ to display the tiny trace of second phase Cu_2S in the sample with x = 0.30 and x = 0.40.

Fig. 2 (a)-(b) Lattice parameters and(c) volume of unit cell as a function of nominal Cu concentration for $In_{2-x}Cu_xS_3$ ($0 \leq x \leq 0.40$).

Fig. 3 (a) Back-scattered electron image for Cu doped β-$In_2S_3$with$x$ = 0.10. (b)-(d) Mappings for the elements In, S and Cu on the polished surface of this representative sample.

Fig.4 Temperature dependence of electrical transport properties (a) Seebeck coefficient; (c) electrical resistivity; (d) power factor for $In_{2-x}Cu_xS_3$($0 \leq x \leq 0.30$) samples.

Fig.5 Temperature dependence of thermal transport properties (a) thermal conductivity (b) lattice thermal conductivity and (c) electrical thermal conductivity for $In_{2-x}Cu_xS_3$($0 \leq x \leq 0.30$) samples.

Fig.6 (a) ZT values as a function of temperature for $In_{2-x}Cu_xS_3$($0 \leq x \leq 0.30$) samples; (b) comparison of ZT_{max} and ZT_{ave} (from 300 to 773 K) for pristine In_2S_3, Mg doped ($In_{1.95}Mg_{0.05}S_3$) and Cu doped ($In_{1.95}Cu_{0.05}S_3$) In_2S_3.

Fig.7 Comparison of thermal conductivities for different elements doped β-In_2S_3samples

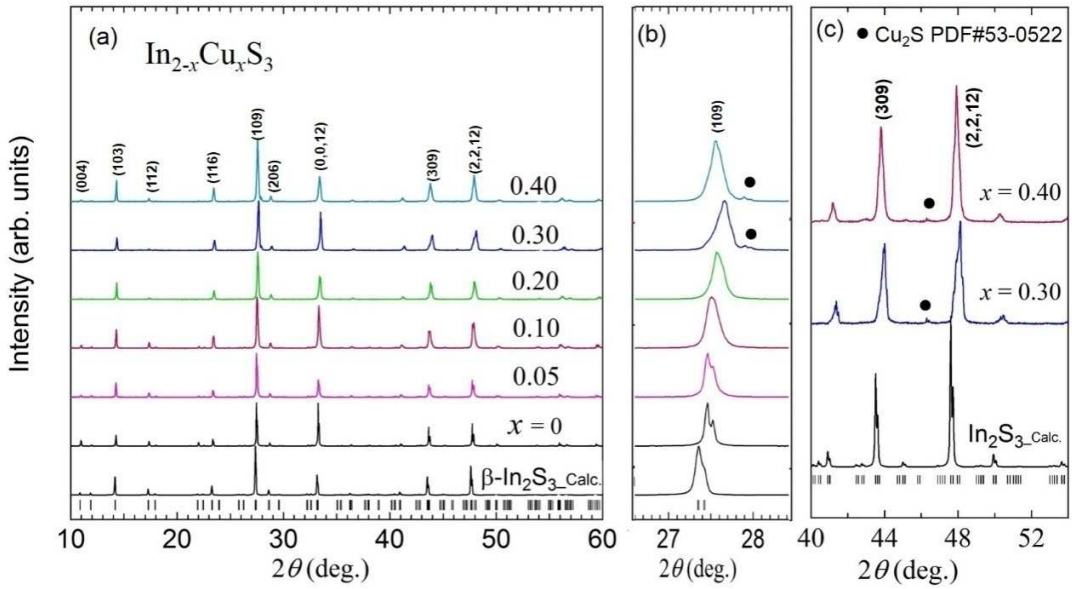

Fig.1

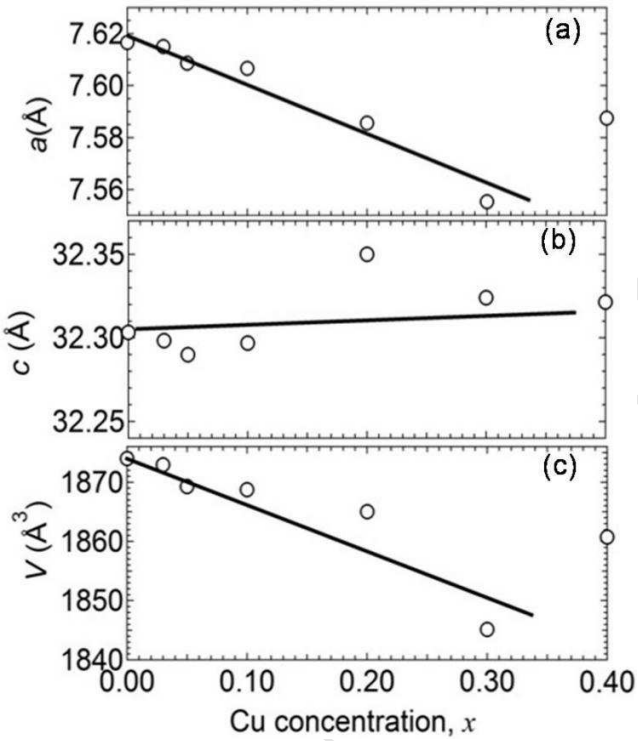

Fig. 2

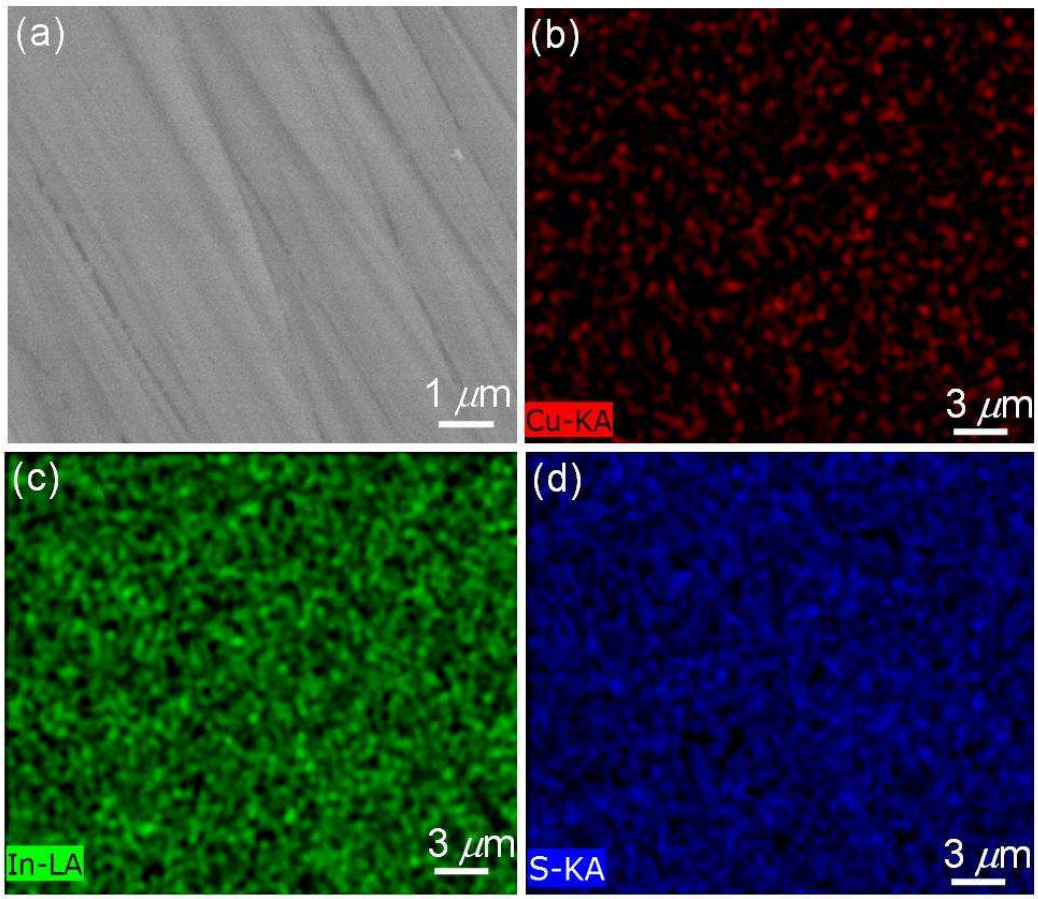

Fig. 3

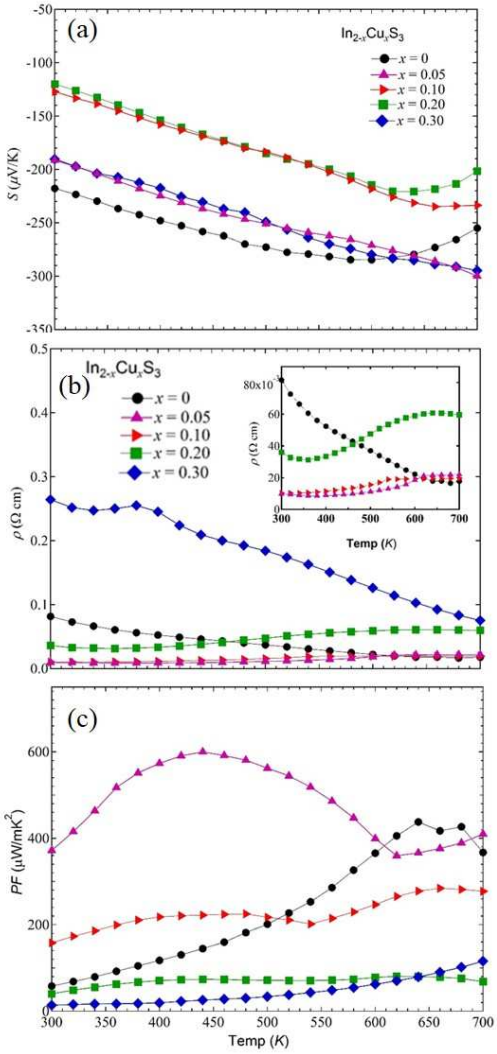
(a)
$In_{2-x}Cu_xS_3$
x = 0
x = 0.05
x = 0.10
x = 0.20
x = 0.30
S (μV/K)
(b)
ρ (Ω cm)
Temp (K)
(c)
PF (μW/mK²)
Temp (K)

Fig. 4

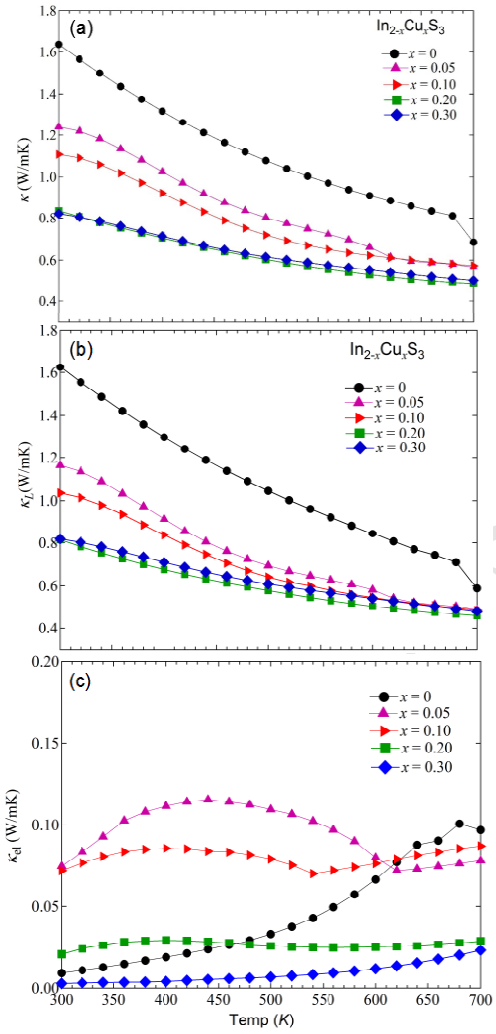
(a)
$In_{2-x}Cu_xS_3$
x = 0
x = 0.05
x = 0.10
x = 0.20
x = 0.30
κ (W/mK)
(b)
$In_{2-x}Cu_xS_3$
x = 0
x = 0.05
x = 0.10
x = 0.20
x = 0.30
$κ_L$(W/mK)
(c)
x = 0
x = 0.05
x = 0.10
x = 0.20
x = 0.30
$κ_{el}$ (W/mK)
Temp (K)

Fig. 5

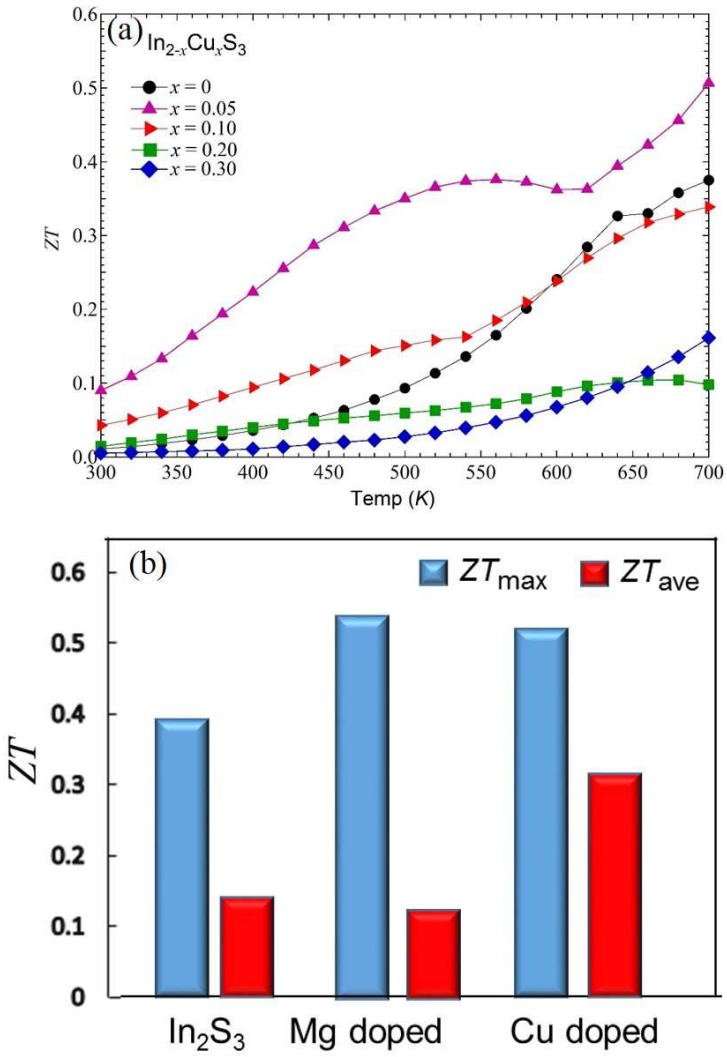
(a) $In_{2-x}Cu_xS_3$
x = 0
x = 0.05
x = 0.10
x = 0.20
x = 0.30
ZT
Temp (K)
(b)
ZT_{max}
ZT_{ave}
ZT
In_2S_3
Mg doped
Cu doped

Fig. 6

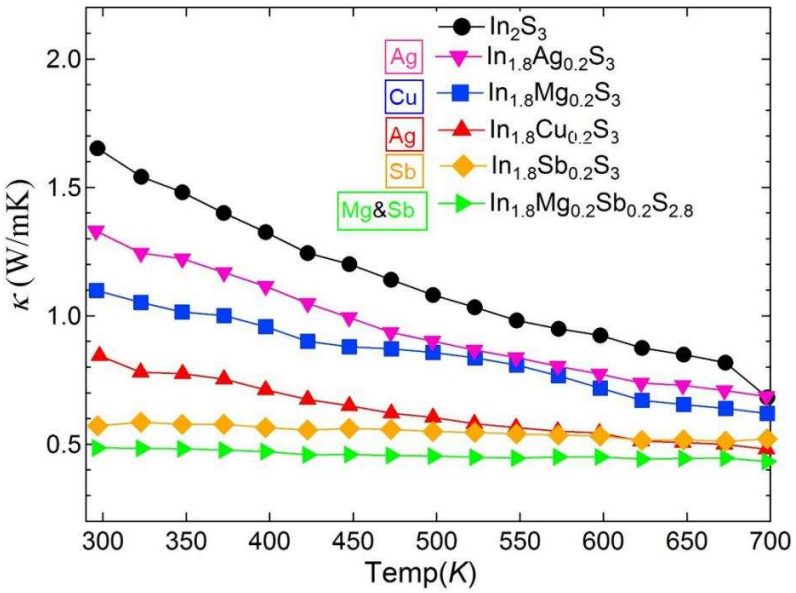

Fig. 7

Table 1 Comparison of pristine β-In_2S_3, Mg doped and Cu doped In_2S_3 room temperature TE properties, ZT_{max} , ZT_{ave}(300 to 700 K). Nominal composition for Mg doped and Cu doped In_2S_3 are$In_{1.95}Mg_{0.05}S_3$ and $In_{1.95}Cu_{0.05}S_3$, respectively.

Sample	$S(\mu VK^{-1})$	$\rho(\Omega cm)$	$PF(\mu Wm^{-1}K^{-2})$	κ($Wm^{-1}K^{-1}$)	$\kappa_L(Wm^{-1}K^{-1})$	ZT_{max}	ZT_{ave}
In_2S_3	218	0.08	58	1.63	1.62	0.38	0.14
Mg doped	246	0.123	49	1.51	1.506	0.53	0.12
Cu doped	191	0.009	372	1.23	1.16	0.51	0.31

β-$In_{2-x}Cu_xS_3$ bulks with high thermoelectric performance were prepared.

Both the electrical resistivity and lattice thermal conductivity reduced after Cu doping.

ZT_{ave} is greatly enhanced after Cu doping.

Cu doping is an efficiently way to optimize the thermoelectric performance of β-In_2S_3.